

## Metal–Organic Frameworks

Isorecticular Expansion of Metal–Organic Frameworks via Pillaring of Metal Templated Tunable Building Layers: Hydrogen Storage and Selective CO<sub>2</sub> CaptureKartik Maity,<sup>[a]</sup> Karabi Nath,<sup>[a]</sup> Michael A. Sinnwell,<sup>[c]</sup> Radha Kishan Motkuri,<sup>[b]</sup> Praveen K. Thallapally,<sup>[c]</sup> and Kumar Biradha\*<sup>[a]</sup>

**Abstract:** The deliberate construction of isorecticular *eea*-metal–organic frameworks (MOFs) (**Cu-*eea*-1**, **Cu-*eea*-2** and **Cu-*eea*-3**) and *rtl*-MOFs (**Co-*rtl*-1** and **Co-*rtl*-2**) has been accomplished based on the ligand-to-axial pillaring of supermolecular building layers. The use of different metal ions resulted in two types of supermolecular building layers (SBLs): Kagome (*kgm*) and square lattices (*sql*) which further interconnect to form anticipated 3D-MOFs. The isorecticular expansion of (3,6)-connected Cu-MOFs has been achieved with desired *eea*-topology based on *kgm* building layers. In addition, two (3,6)-connected Co-*rtl*-MOFs were also successfully constructed based on *sql* building layers. The Cu-*eea*-MOFs were shown to act as hydrogen storage materials with appreciable amount of hydrogen uptake abilities. Moreover Cu-*eea*-MOFs have also exhibited remarkable CO<sub>2</sub> capture ability at ambient condition compared to nitrogen and methane, due to the presence of amide functionalities.

Metal–organic frameworks (MOFs) have grown rapidly as effective porous materials in the last couple of decades due to their utility in various applications.<sup>[1–8]</sup> The MOFs provide a unique advantage for the introduction of desired functionalities, and therefore properties, by the judicious selection of appropriate organic building block prior to assembly of the components. The substantial challenge of reticular chemistry is associated with the synthesis of crystalline materials using appropriate organic linkers for connecting symmetrical secondary building units (SBUs) into extended frameworks with predefined topologies. For such isorecticular synthesis of series of MOFs, the ri-

gidity and symmetry of the organic linkers should be maintained while increasing the size of the linkers. In addition, the reaction conditions play a significant role in obtaining series of isorecticular MOFs as the formation of the same inorganic SBUs is essential.<sup>[9–13]</sup> The first series of isorecticular MOFs were produced by connecting octahedral-shaped inorganic SBUs through various linear di-carboxylate linkers to produce 16 compounds with identical topologies. These MOFs were found to exhibit high methane and hydrogen storage capacity.<sup>[9]</sup>

The paddlewheel cluster M<sub>2</sub>(COO)<sub>4</sub> is one of the most common SBUs that has been observed to form with a wide range of metal ions. This binuclear metal cluster can act as a square building unit, as well as an octahedral building unit depending upon the nature of the polytopic ligands. Kagome lattice (*kgm*) and square lattice (*sql*) are the two edge transitive 2D-nets, which can be generated from a square building unit.<sup>[14–20]</sup> Pillaring of these 2D-layered nets containing paddlewheel units into a 3D-porous architecture has been studied recently and the approach has been termed as supermolecular building layers (SBLs). Pillaring methods of SBLs involve several strategies which include linking axial-to-axial (A-A), ligand-to-ligand (L-L) and ligand-to-axial (L-A). Recently amide and amine functionalized 3-connected organic ligands have been shown to form Cu-MOFs with *eea* and *rtl* topology, respectively, based on the L-A pillaring strategy. These Cu-MOFs were explored for CO<sub>2</sub> capture ability and hydrocarbon separations.<sup>[18]</sup>

Design and synthesis of porous MOFs is of importance for gas storage and separation purposes, impacting day-to-day aspects of society, such as environmental protection and energy utilization. In particular, the capture of carbon dioxide from the atmosphere is a necessity to minimize the greenhouse effect, and the storage of hydrogen and methane gases is absolutely crucial for the global utilization of clean energy.<sup>[21,22]</sup> For the last few decades, the world's flourishing energy demand is being furnished by the combustion of fossil fuels, resulting in an ever increasing CO<sub>2</sub> concentration in the atmosphere.<sup>[23–34]</sup> The combined effect of CO<sub>2</sub> emission on climate, and an inadequate supply of fossil fuels have prompted the development of alternative fuel sources. Hydrogen is considered as one of the more favourable energy sources for the replacement of coal and gasoline, due to its high gravimetric heat of combustion and zero carbon emission. Therefore, the use of hydrogen as fuel, for automobiles and various other purposes, necessitates the exploration of hydrogen storage materials.<sup>[35–38]</sup>

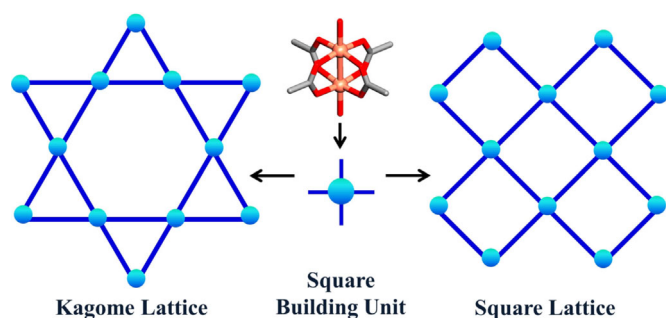
[a] Dr. K. Maity, K. Nath, Prof. K. Biradha  
Department of Chemistry, Indian Institute of Technology  
Kharagpur 721302 (India)  
E-mail: kbiradha@chem.iitkgp.ernet.in

[b] Dr. R. K. Motkuri  
Energy and Environment Directorate  
Pacific Northwest National Laboratory, Richland, WA 99352 (USA)

[c] Dr. M. A. Sinnwell, Dr. P. K. Thallapally  
Physical and Computational Sciences Directorate  
Pacific Northwest National Laboratory, Richland, WA 99352 (USA)

 Supporting information and the ORCID identification number(s) for the author(s) of this article can be found under:  
<https://doi.org/10.1002/chem.201902491>.

In this contribution, the gradual expansion of the frameworks has been achieved for an isotreticular series of Cu-MOFs by maintaining the underlying *eea*-topology. The isophthalate moieties of the ligands form the anticipated 2D-layers with *kgm*-topology (Scheme 1) in combination with the metal pad-

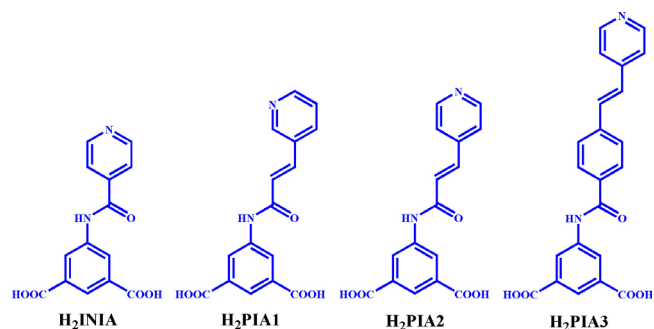


**Scheme 1.** Two possible edge transitive 2D-nets from square building unit: Kagome and square lattice.

dlewheel, whereas the pyridyl group, a second functionality, connects the adjacent layers to lead to the formation of (3,6)-connected 3D-MOFs. Further the use of  $\text{Co}^{\text{II}}$  salt instead of  $\text{Cu}^{\text{II}}$  salt resulted in the formation of *sql* building layers. The resulting Cu-*eea*-MOFs have been explored for selective capture of  $\text{CO}_2$  over nitrogen and methane. Further the Cu-MOFs were also found to exhibit remarkable hydrogen storage capability. However the  $\text{Co}^{\text{II}}$ -based *rtl* MOFs hardly showed porous nature, possibly due to collapse of the pores in one case and the presence of interpenetration that totally occupied the voids in another case.

The organic building units used in this work (Scheme 2) are the elongated version of the previously explored T-shaped ligand, 5-(isonicotinamido) isophthalic acid ( $\text{H}_2\text{INIA}$ ).<sup>[16,18]</sup> The ligands, 5-(3-(pyridin-3-yl)acrylamido)isophthalic acid ( $\text{H}_2\text{PIA1}$ ), 5-(3-(pyridin-4-yl)acrylamido)isophthalic acid ( $\text{H}_2\text{PIA2}$ ) and 5-(4-(2-(pyridin-4-yl)vinyl)benzamido)isophthalic acid ( $\text{H}_2\text{PIA3}$ ) were synthesized by condensation reactions of dimethyl-5-aminoisophthalate with 3-pyridylacrylic acid, 4-pyridylacrylic acid and 4-(2-(pyridin-4-yl)vinyl)benzoic acid, respectively, followed by hydrolysis. The synthesized molecules were characterized by  $^1\text{H}$  NMR spectroscopy prior to their use for MOFs synthesis.

The solvothermal reaction of copper nitrate and  $\text{H}_2\text{PIA1}$  in a DMF-EtOH- $\text{H}_2\text{O}$  solvent mixture resulted in needle-shaped



**Scheme 2.** Molecular structure of the organic building blocks.

green coloured single crystals of Cu-MOF. The crystal structure of the as synthesized MOF was confirmed by single-crystal X-ray diffraction and has been formulated as  $\{[(\text{PIA1})_6\text{Cu}_6](\text{solv.})_x\}_n$  (**Cu-*eea*-1**). The structural analysis revealed that **Cu-*eea*-1** crystallised in the  $R\bar{3}$  space group and the asymmetric unit contains one unit each of PIA1 and  $\text{Cu}^{\text{II}}$  ions. The  $\text{Cu}^{\text{II}}$  ion was found to exhibit a distorted square pyramidal coordination geometry and two such types of square pyramidal  $\text{Cu}^{\text{II}}$  centre produce the  $\text{Cu}_2(\text{COO})_4$  paddlewheel SBU. The  $\text{Cu}^{\text{II}}$  centres of the dinuclear  $\text{Cu}_2$ -paddlewheel are equatorial coordinated by four carboxylate oxygen atoms and the pyridyl nitrogen from two different ligands occupied two apical positions.

The isophthalate moieties in **Cu-*eea*-1** are involved in bridging of the square building  $\text{Cu}_2$ -paddlewheel in order to produce 2D-*kgm* layers. Further these 2D-*kgm* layers are interconnected by the pyridyl moieties through the L-A pillaring method to produce a porous 3D-framework. The PIA1 unit with a T-shaped geometry acts as a 3-connected node, whereas the  $\text{Cu}_2$ -paddlewheel serves as a 6-connected node to form a (3,6)-connected framework with the desired *eea*-topology. The pillaring of the *kgm*-layers occurs in such a way that the six-membered ring window of a layer interconnects two three-membered ring windows from the adjacent *kgm*-sheets to generate a large and prolate-ellipsoid-shaped Cage A. Further in between a pair of Cage A, another type of cage has been formed by the connection between a pair of three-membered ring windows from the adjacent two layers, which is more spherical in nature (cage B). Cage A is encircled by six PIA1 units and twelve  $\text{Cu}_2$ -paddlewheel clusters (length 26 Å), whereas Cage B is surrounded by six  $\text{Cu}_2$ -paddlewheel clusters and six PIA1 units (length  $\approx$  16 Å, width  $\approx$  12 Å) (Figure 1).

It has been observed that size of the cavities and the separation between the *kgm*-layers are larger in **Cu-*eea*-1** compared to the previously studied Cu-based (**Cu-INIA**) *eea*-MOF, constructed by using INIA. As our aim was to build a series of *eea*-MOFs with reticular expansion of the framework, so another

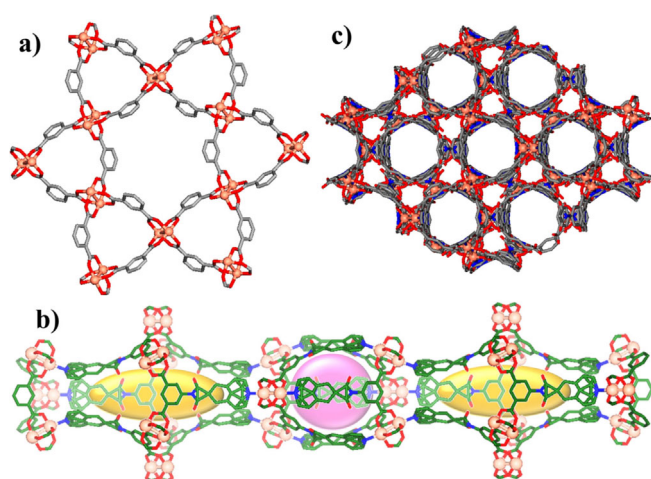


**Figure 1.** Illustrations for Cu-*eea*-MOFs: a) *kgm*-layers formed by the isophthalate moieties; b) two types of cages: cage A (yellow, prolate-ellipsoid shaped) and cage B (pink, spherical); c) overall (3,6)-connected MOF with *eea*-topology.

couple of ligands were designed, H<sub>2</sub>PIA2 and H<sub>2</sub>PIA3, by shifting the position of N-donor coordination sites of the pyridine ring, and also increasing the length of the spacer between isophthalate and pyridyl moieties. The solvothermal reaction of H<sub>2</sub>PIA2 and H<sub>2</sub>PIA3 with copper nitrate in DMF/acetic acid solvent system afforded block-shaped green coloured single crystals of the corresponding Cu-MOFs. The crystal structures were determined by single-crystal X-ray diffraction and the formulas were found to be  $\{[(\text{PIA}2)_6\text{Cu}_6](\text{solv.})_x\}_n$  (**Cu-eea-2**) and  $\{[(\text{PIA}3)_6\text{Cu}_6](\text{solv.})_x\}_n$  (**Cu-eea-3**).

As anticipated the two expanded MOFs, **Cu-eea-2** and **Cu-eea-3** were found to be isoreticular with the previous one, having *eea*-topology. The sizes of the two types of cages have also been found to increase. The crystallographic parameters revealed a gradual increase of *c*-axis length compared to the earlier synthesized *eea*-MOF as: 37.8 Å (**Cu-INIA**), 42.6 Å (**Cu-eea-1**), 44.7 Å (**Cu-eea-2**) and 52.2 Å (**Cu-eea-3**). As the length of the middle spacer for the ligands were increased, the separation between the *kgm*-layers have been also found to be increased (Figure 2). The inter-layer distances between the two successive *kgm*-layers are 12.67 Å (**Cu-INIA**), 14.19 Å (**Cu-eea-1**), 14.89 Å (**Cu-eea-2**) and 17.42 Å (**Cu-eea-3**).

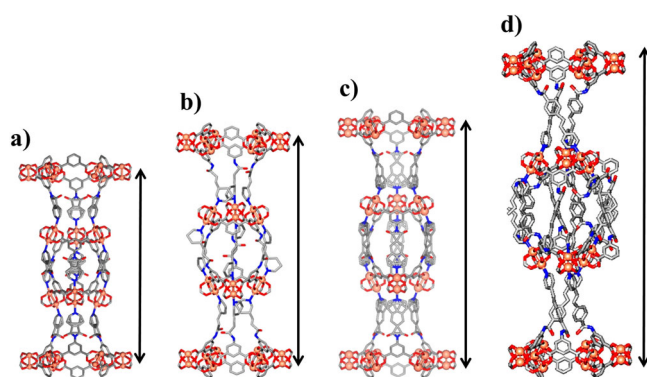


**Figure 2.** Gradual expansion of the cavity sizes as well as separation between the *kgm*-layers in a) **Cu-INIA**; b) **Cu-eea-1**; c) **Cu-eea-2**; d) **Cu-eea-3**.

As discussed earlier, the square building unit has an ability to generate *sql* SBL other than the *kgm*-sheet; these organic building units were further employed to construct MOFs with another transition metal in order to explore the versatility of the SBL approach. The solvothermal reaction of H<sub>2</sub>PIA2 with cobalt nitrate in DMA-H<sub>2</sub>O solvent system afforded dark purple coloured block-shaped single crystals. The crystal structure was determined by single crystal X-ray diffraction, and the MOF has been formulated as  $\{[(\text{PIA}2)_2\text{Co}_2](\text{solv.})_x\}_n$  (**Co-rtl-1**). The structural analysis revealed that **Co-rtl-1** crystallised in *P2<sub>1</sub>/c* space group and the asymmetric unit contains one unit each of Co<sup>II</sup> and PIA2 ions. Co<sup>II</sup> ions exhibited a distorted square-pyramidal geometry with four equatorial positions coordinated by carboxylates and the apical position being occupied by the pyridyl moiety. Two such penta-coordinated Co<sup>II</sup> centres produced a Co<sub>2</sub>-paddlewheel cluster in a similar fashion as in Cu-*eea* MOFs.

Interestingly, the square building unit, Co<sub>2</sub>-paddlewheel cluster preferred the formation of *sql*-layers through isophthalate

linkers, over the *kgm*-sheet observed in Cu-*eea* MOFs. In this case the *sql*-layers are also interconnected through the pyridyl coordination in an L-A pillaring mode to produce 3D-frameworks. The overall 3D-network was found to have a (3,6)-connected *rtl*-topology, where the ligand acted as a 3-connected node and the Co<sub>2</sub>-paddlewheel as 6-connected node. The square windows from *sql*-layers are comprised of four isophthalate units; the adjacent pairs of benzene moieties point up, while the other two benzene moieties point down. The distances between two successive *sql*-layers was found to be 13.6 Å and pillaring of the *sql*-layers generates a rectangular grid-type cage with the dimension of approximately 10×10×13.6 Å (Figure 3).

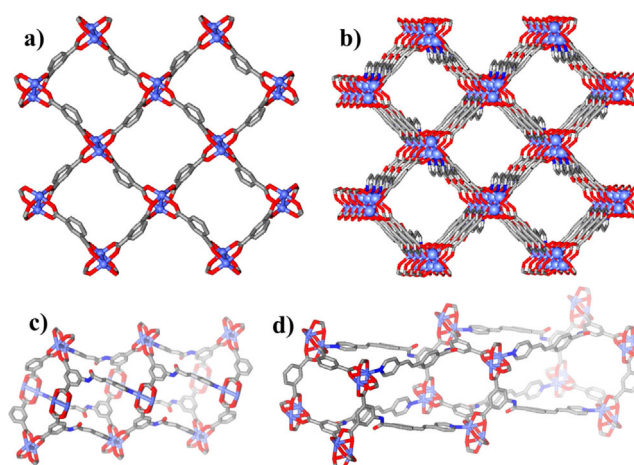


**Figure 3.** Illustrations for **Co-rtl-1**: a) *sql*-layers formed by the isophthalate moieties; b) overall (3,6)-connected MOF with *rtl*-topology; side view of the rectangular grid type cage; c) **Co-rtl-1**; d) **Co-rtl-2**.

The ligand H<sub>2</sub>PIA3 was employed along with cobalt(II) salts for the construction of desired *rtl*-MOFs, anticipating the increase in size of the cages as for the Cu-*eea* MOFs series. The solvothermal reaction of H<sub>2</sub>PIA3 and cobalt nitrate in DMF-EtOH-H<sub>2</sub>O resulted in deep-purple coloured block-shaped crystals. The single-crystal X-ray diffraction analysis revealed the space group was *P2<sub>1</sub>/c* and the asymmetric unit was composed of one unit each of Co<sup>II</sup> and PIA3 ions, with the formula  $\{[(\text{PIA}3)_2\text{Co}_2](\text{solv.})_x\}_n$  (**Co-rtl-2**). Further structural analysis showed that **Co-rtl-2** exhibited a (3,6)-connected two-fold interpenetrated 3D-framework with *rtl*-topology. The desired expansion in terms of size of the cage (dimension approximately 10×10×20 Å) was achieved, but the huge voids of the frameworks were occupied by the two-fold interpenetration of the networks. The interlayer separation of *sql*-layers within the *rtl*-framework was found to be ≈ 20 Å (Figure 3).

The permanent porosities of Cu-*eea* MOFs were investigated by nitrogen isotherms at 77 K for the activated phase of those MOFs. The nitrogen uptake of **Cu-eea-1** exhibited an adsorption isotherm with an unusual stepwise uptake, which led to generation of a prominent hysteresis between the adsorption and desorption curves, and which may be due to the flexibility of the frameworks. The amount of nitrogen uptake up to the

first step was found to be  $\approx 219 \text{ cm}^3 \text{ g}^{-1}$ , whereas the total amount of nitrogen adsorption by the framework at 1 bar was  $\approx 278 \text{ cm}^3 \text{ g}^{-1}$ . The Brunauer–Emmett–Teller (BET) surface area for **Cu-eea-1** was estimated to be  $687 \text{ m}^2 \text{ g}^{-1}$ . Further the nitrogen adsorption isotherms for **Cu-eea-2** and **Cu-eea-3** were also measured and the corresponding BET surface areas were found to be 873 and  $922 \text{ m}^2 \text{ g}^{-1}$  respectively, with reversible type-I isotherms. A small hysteresis was observed in the case of **Cu-eea-2**, due to the presence of a slight plateau in the desorption isotherm (Figure 4). We note here that the framework of **Co-rtl-1** was found to collapse during the activation process, and it hardly showed any kind of porous behaviour. The presence of two-fold interpenetration in **Co-rtl-2** makes it a non-porous material.

All the MOFs, **Cu-eea-1**, **Cu-eea-2** and **Cu-eea-3**, were analysed for their ability towards the storage of hydrogen at ambient pressure. **Cu-eea-1** was found to be capable of storing  $142 \text{ cm}^3 \text{ g}^{-1}$  (1.27 wt.%) of hydrogen at 77 K and one bar pressure without any sort of hysteresis in adsorption and desorption isotherms, in contrast to its nitrogen adsorption isotherm. The other two MOFs, **Cu-eea-2** and **Cu-eea-3**, also exhibited a significant amount of hydrogen uptake capacity of  $180 \text{ cm}^3 \text{ g}^{-1}$  (1.61 wt.%) and  $202 \text{ cm}^3 \text{ g}^{-1}$  (1.8 wt.%), respectively, at 77 K and ambient pressure. It can be concluded that the change in position of pyridyl nitrogen, and also the expansion of the spacer, led to the increase in the hydrogen uptake values (Figure 4). The hydrogen storage capabilities exhibited by these MOFs are comparable with some of the highly porous MOFs which include IRMOF-6, MOF-177 and PCN-68. (Table S3, Supporting Information)

Apart from the hydrogen storage ability, these materials were explored for their  $\text{CO}_2$  capture ability due to the presence of amide-decorated cages and channels within the network of the MOFs. As anticipated, the **Cu-eea-1**, **Cu-eea-2** and **Cu-eea-3** have shown remarkable  $\text{CO}_2$  capture ability at ambient conditions, along with gradual increases in adsorption values as the pore size increases. The MOF containing smaller cavities, **Cu-eea-1** can uptake  $105 \text{ cm}^3 \text{ g}^{-1}$  of  $\text{CO}_2$  whereas **Cu-eea-2** with somewhat bigger cavities showed better  $\text{CO}_2$  uptake capacity ( $114 \text{ cm}^3 \text{ g}^{-1}$ ) at 273 K and 1 bar pressure. Further **Cu-eea-3**, with larger cages and channels compared to the other two, can capture  $143 \text{ cm}^3 \text{ g}^{-1}$  of  $\text{CO}_2$  which was found to be the highest among the present Cu-*eea*-MOFs (Figure 4). The  $\text{CO}_2$  uptake capacities for the present MOFs are comparable with some of the previously explored Cu-based MOFs for  $\text{CO}_2$  capture (e.g., JUC-1000:  $125 \text{ cm}^3 \text{ g}^{-1}$ ; Cu-NTTA:  $115.6 \text{ cm}^3 \text{ g}^{-1}$ ; LIFM-10:  $129.5 \text{ mL g}^{-1}$ ; LIFM-11:  $129.5 \text{ mL g}^{-1}$ ).<sup>[5,30,16,33]</sup> (Table S2, Supporting Information) The adsorption enthalpies ( $Q_{st}$ ) for  $\text{CO}_2$  adsorption were found to be 27.5, 36 and  $17.7 \text{ kJ mol}^{-1}$  for **Cu-eea-1**, **Cu-eea-2** and **Cu-eea-3**, respectively, at zero coverage.

The selective capture of  $\text{CO}_2$  over nitrogen at ambient temperature and pressure was analysed for all the Cu-*eea* MOFs given their practical importance in removal of  $\text{CO}_2$  from flue gas (mixture of  $\text{N}_2$  and  $\text{CO}_2$ ) produced in the coal-fired power plants. All the MOFs were found to exhibit significant  $\text{CO}_2$  uptake capacity at ambient condition, whereas they hardly adsorb nitrogen under similar conditions. **Cu-eea-1** was found to adsorb  $4 \text{ cm}^3 \text{ g}^{-1}$  of nitrogen at 298 K and 1 atm pressure, whereas it can capture about  $66.9 \text{ cm}^3 \text{ g}^{-1}$  of  $\text{CO}_2$  at the same

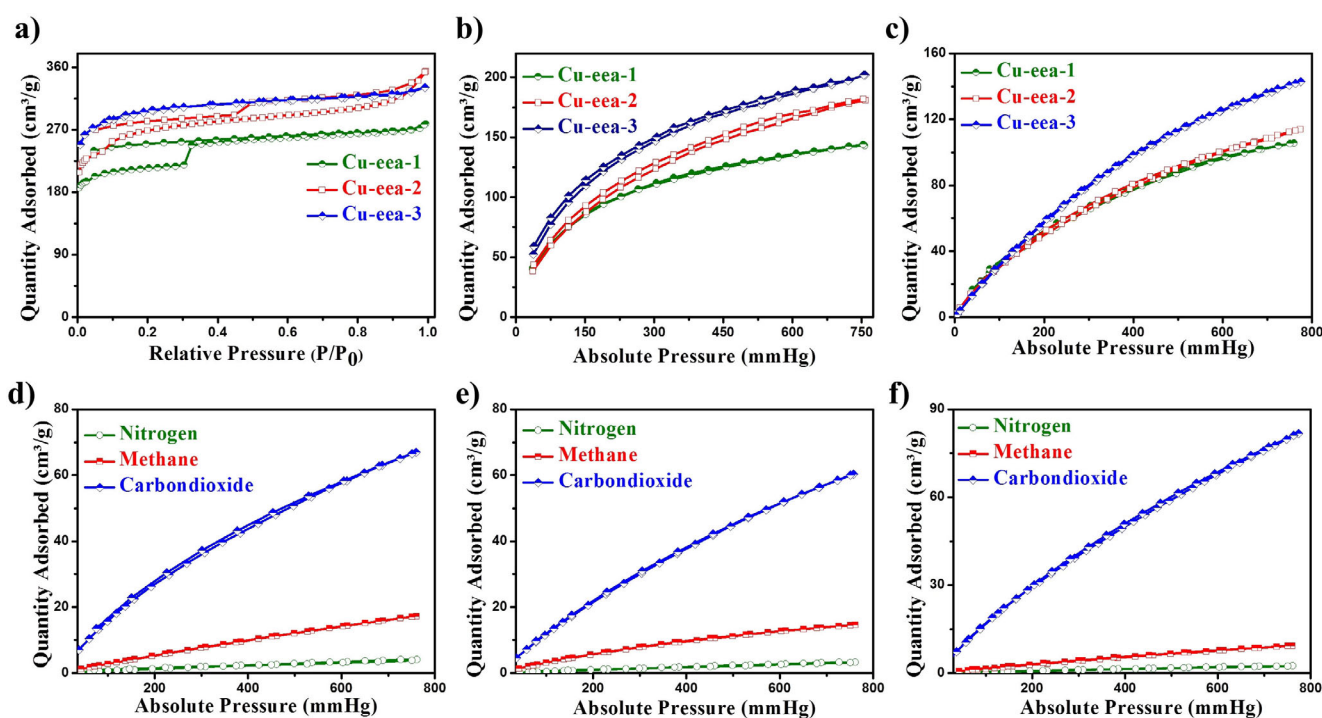


**Figure 4.** a) Nitrogen isotherm for Cu-*eea* MOFs at 77 K and 1 bar pressure; b) hydrogen uptake isotherm for the Cu-*eea* MOFs at 77 K and 1 bar; c)  $\text{CO}_2$  adsorption isotherms for the Cu-*eea* MOFs at 273 K and 1 bar; Selective adsorption of  $\text{CO}_2$  over nitrogen and methane at ambient conditions (298 K and 1 bar pressure): d) **Cu-eea-1**; e) **Cu-eea-2**; f) **Cu-eea-3**.

conditions. The other two MOFs have also exhibited similar behaviour as **Cu-*eea-2*** and **Cu-*eea-3*** were found to uptake 60 and 81.7 cm<sup>3</sup>g<sup>-1</sup> of CO<sub>2</sub> at 298 K and 1 atm pressure, respectively, but they exhibited little nitrogen adsorption ability under the same conditions (3.2 and 2.4 cm<sup>3</sup>g<sup>-1</sup>). The adsorption selectivity was also maintained at 273 K as the Cu-*eea*-MOFs adsorbed a lesser amount of nitrogen (10, 7 and 4 cm<sup>3</sup>g<sup>-1</sup>, respectively) compared to CO<sub>2</sub> (105, 114 and 143 cm<sup>3</sup>g<sup>-1</sup>, respectively) (Figure 4).

Further, Cu-*eea*-MOFs were also analysed for their methane adsorption propensity at ambient conditions. The methane adsorption isotherm revealed that the Cu-*eea* MOFs have very little tendency towards its storage. The Cu-*eea* MOFs were found to uptake 17, 14 and 9 cm<sup>3</sup>g<sup>-1</sup> of methane, respectively, at 298 K and 1 bar pressure which are much less than the amounts of CO<sub>2</sub> adsorbed (66.9, 60, and 81.7 cm<sup>3</sup>g<sup>-1</sup>) at the same conditions. The methane adsorption studies were also carried out at 288 and 278 K, but did not show much improvement in adsorption values. At 278 K and 1 bar pressure the amounts of methane adsorbed were found to be 25.8, 26.1 and 13.2 cm<sup>3</sup>g<sup>-1</sup>, respectively, whereas the methane uptake capacities were 24.6, 20.8 and 13.6 cm<sup>3</sup>g<sup>-1</sup> at 288 K and 1 bar pressure (Figure 4). The adsorption selectivity of Cu-*eea* MOFs towards CO<sub>2</sub> over CH<sub>4</sub> is very important in the removal of unwanted CO<sub>2</sub> from landfill gases, which contain about 50% CO<sub>2</sub>.

In summary, three elongated trigonal ligands were designed and synthesized successfully for the deliberate construction of isorecticular (3,6)-connected Cu-*eea* MOFs and Co-*rtl* MOFs, based on the supermolecular building layer approach. The ligands utilized here for the MOFs synthesis contain larger spacers compared to previously explored ones, and consequently the gradual expansion of framework dimensions has been achieved for the desired MOFs whilst retaining the underlying *eea*-topology. Further the change of metal ions from Cu<sup>II</sup> to Co<sup>II</sup> resulted in the construction of (3,6)-connected interpenetrated and non-interpenetrated Co-*rtl* MOFs. The amide-decorated isorecticular Cu-*eea* MOFs exhibit remarkable and selective CO<sub>2</sub> capture ability at ambient conditions. **Cu-*eea-3*** can uptake a significant amount of CO<sub>2</sub> at 273 K and 1 bar pressure, and the uptake is comparable with recently reported highly porous MOFs used for CO<sub>2</sub> capture purpose. However, all these MOFs hardly adsorbed nitrogen and methane at ambient conditions, which can be utilized for the separation of CO<sub>2</sub> from the mixture of CO<sub>2</sub>/N<sub>2</sub> and CO<sub>2</sub>/CH<sub>4</sub>. Moreover, the Cu-based MOFs were also found to exhibit remarkable hydrogen storage ability. The hydrogen uptake capacities of these *eea*-MOFs are comparable with some of the earlier explored well known porous MOFs.

## Experimental Details

Full details of synthesis and characterisation of the ligands and MOFs can be found in the Supporting Information.

CCDC 1918819, 1918820, 1918821, 1918822, and 1918823 contain the supplementary crystallographic data for this paper. These data are provided free of charge by The Cambridge Crystallographic Data Centre.

## Acknowledgements

We acknowledge SERB (EMR/2017/001499), New Delhi, India, for financial support and DST-FIST for the single-crystal X-ray diffractometer. K.M. thanks UGC and IIT Kharagpur for research fellowship.

## Conflict of interest

The authors declare no conflict of interest.

**Keywords:** CO<sub>2</sub> capture · hydrogen storage · isorecticular · metal-organic frameworks · supermolecular building layers

- [1] H.-C. Zhou, J. R. Long, O. M. Yaghi, *Chem. Rev.* **2012**, *112*, 673–674.
- [2] P. Nugent, Y. Belmabkhout, S. D. Burd, A. J. Cairns, R. Luebke, K. Forrester, T. Pham, S. Ma, B. Space, L. Wojtas, M. Eddaoudi, M. J. Zaworotko, *Nature* **2013**, *495*, 80–84.
- [3] J. Lee, O. K. Farha, J. Roberts, K. A. Scheidt, S. T. Nguyen, J. T. Hupp, *Chem. Soc. Rev.* **2009**, *38*, 1450–1459.
- [4] H.-C. Zhou, S. Kitagawa, *Chem. Soc. Rev.* **2014**, *43*, 5415–5418.
- [5] H. He, Q. Sun, W. Gao, J. A. Perman, F. Sun, G. Zhu, B. Aguilá, K. Forrester, B. Space, S. Ma, *Angew. Chem. Int. Ed.* **2018**, *57*, 4657–4662; *Angew. Chem.* **2018**, *130*, 4747–4752.
- [6] B. Chen, S. Xiang, G. Qian, *Acc. Chem. Res.* **2010**, *43*, 1115–1124.
- [7] M. Eddaoudi, J. Kim, J. B. Wachter, H. K. Chae, M. O’Keeffe, O. M. Yaghi, *J. Am. Chem. Soc.* **2001**, *123*, 4368–4369.
- [8] B. Moulton, J. Lu, A. Mondal, M. J. Zaworotko, *Chem. Commun.* **2001**, 863–864.
- [9] M. Eddaoudi, J. Kim, N. Rosi, D. Vodak, J. Wachter, M. O’Keeffe, O. M. Yaghi, *Science* **2002**, *295*, 469–472.
- [10] S. Surlblé, C. Serre, C. Mellot-Draznieks, F. Millange, G. Férey, *Chem. Commun.* **2006**, 284–286.
- [11] V. Colombo, C. Montoro, A. Maspero, G. Palmisano, N. Masciocchi, S. Galli, E. Barea, J. A. R. Navarro, *J. Am. Chem. Soc.* **2012**, *134*, 12830–12843.
- [12] H. Furukawa, Y. B. Go, N. Ko, Y. K. Park, F. J. Uribe-Romo, J. Kim, M. O’Keeffe, O. M. Yaghi, *Inorg. Chem.* **2011**, *50*, 9147–9152.
- [13] F. Moreau, D. I. Kolokolov, A. G. Stepanov, T. L. Easun, A. Dailly, W. Lewis, A. J. Blake, H. Nowell, M. J. Lennox, E. Besley, S. Yang, M. Schröder, *Proc. Natl. Acad. Sci. USA* **2017**, *114*, 3056–3061.
- [14] J. F. Eubank, L. Wojtas, M. R. Hight, T. Bousquet, V. C. Kravtsov, M. Eddaoudi, *J. Am. Chem. Soc.* **2011**, *133*, 17532–17535.
- [15] A. Schoedel, W. Boyette, L. Wojtas, M. Eddaoudi, M. J. Zaworotko, *J. Am. Chem. Soc.* **2013**, *135*, 14016–14019.
- [16] Y. Xiong, Y. Z. Fan, R. Yang, S. Chen, M. Pan, J. J. Jiang, C. Y. Su, *Chem. Commun.* **2014**, *50*, 14631–14634.
- [17] L. Du, S. Yang, L. Xu, H. Mina, B. Zheng, *CrystEngComm* **2014**, *16*, 5520–5523.
- [18] Z. Chen, K. Adil, L. J. Weselinski, Y. Belmabkhout, M. Eddaoudi, *J. Mater. Chem. A* **2015**, *3*, 6276–6281.
- [19] O. Benson, I. da Silva, S. P. Argent, R. Cabot, M. Savage, H. G. W. Godfrey, Y. Yan, S. F. Parker, P. Manuel, M. J. Lennox, T. Mitra, T. L. Easun, W. Lewis, A. J. Blake, E. Besley, S. Yang, M. Schröder, *J. Am. Chem. Soc.* **2016**, *138*, 14828–14831.
- [20] Y. Xiong, Y.-Z. Fan, D. D. Borges, C.-X. Chen, Z.-W. Wei, H.-P. Wang, M. Pan, J.-J. Jiang, G. Maurin, C.-Y. Su, *Chem. Eur. J.* **2016**, *22*, 16147–16156.
- [21] H. Li, K. Wang, Y. Sun, C. T. Lollar, J. Li, H.-C. Zhou, *Mater. Today* **2018**, *21*, 108–121.
- [22] C. E. Wilmer, O. K. Farha, Y.-S. Bae, J. T. Hupp, R. Q. Snurr, *Energy Environ. Sci.* **2012**, *5*, 9849–9856.
- [23] Z. Zhang, Y. Zhao, Q. Gong, Z. Li, J. Li, *Chem. Commun.* **2013**, *49*, 653–661.
- [24] J. A. Mason, T. M. McDonald, T. H. Bae, J. E. Bachman, K. Sumida, J. J. Dutton, S. S. Kaye, J. R. Long, *J. Am. Chem. Soc.* **2015**, *137*, 4787–4803.

- [25] L. Liang, C. Liu, F. Jiang, Q. Chen, L. Zhang, H. Xue, H.-L. Jiang, J. Qian, D. Yuan, M. Hong, *Nat. Commun.* **2017**, *8*, 1233–1242.
- [26] R. Banerjee, A. Phan, B. Wang, C. Knobler, H. Furukawa, M. O’Keeffe, O. M. Yaghi, *Science* **2008**, *319*, 939–943.
- [27] S. D. Burd, S. Ma, J. A. Perman, B. J. Sikora, R. Q. Snurr, P. K. Thallapally, J. Tian, L. Wojtas, M. J. Zaworotko, *J. Am. Chem. Soc.* **2012**, *134*, 3663–3666.
- [28] K. Sumida, D. L. Rogow, J. A. Mason, T. M. McDonald, E. D. Bloch, Z. R. Herm, T.-H. Bae, J. R. Long, *Chem. Rev.* **2012**, *112*, 724–781.
- [29] B. Zheng, J. Bai, J. Duan, L. Wojtas, M. J. Zaworotko, *J. Am. Chem. Soc.* **2011**, *133*, 748–751.
- [30] X. Guo, Z. Zhou, C. Chen, J. Bai, C. He, C. Duan, *ACS Appl. Mater. Interfaces* **2016**, *8*, 31746–31756.
- [31] S. Nandi, S. Collins, D. Chakraborty, D. Banerjee, P. K. Thallapally, T. K. Woo, R. Vaidyanathan, *J. Am. Chem. Soc.* **2017**, *139*, 1734–1737.
- [32] P. Chandrasekhar, A. Mukhopadhyay, G. Savitha, J. N. Moorthy, *J. Mater. Chem. A* **2017**, *5*, 5402–5412.
- [33] J. Jiang, Z. Lu, M. Zhang, J. Duan, W. Zhang, Y. Pan, J. Bai, *J. Am. Chem. Soc.* **2018**, *140*, 17825–17829.
- [34] M. L. Foo, R. Matsuda, Y. Hijikata, R. Krishna, H. Sato, S. Horike, A. Hori, J. G. Duan, Y. Sato, Y. Kubota, M. Takata, S. Kitagawa, *J. Am. Chem. Soc.* **2016**, *138*, 3022–3030.
- [35] B. Chen, N. W. Ockwig, A. R. Millward, D. S. Contreras, O. M. Yaghi, *Angew. Chem. Int. Ed.* **2005**, *44*, 4745–4749; *Angew. Chem.* **2005**, *117*, 4823–4827.
- [36] O. K. Farha, A. M. Spokoyny, K. L. Mulfort, M. F. Hawthorne, C. A. Mirkin, J. T. Hupp, *J. Am. Chem. Soc.* **2007**, *129*, 12680–12681.
- [37] M. P. Suh, H. J. Park, T. K. Prasad, D. W. Lim, *Chem. Rev.* **2012**, *112*, 782–835.
- [38] M. Dincă, J. R. Long, *J. Am. Chem. Soc.* **2005**, *127*, 9376–9377.

---

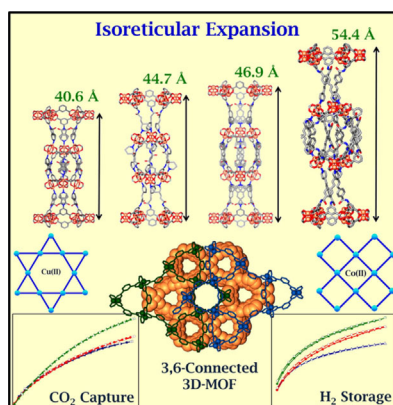
Manuscript received: May 31, 2019

Accepted manuscript online: September 6, 2019

Version of record online: ■ ■ ■ 0000

## COMMUNICATION

**Pillar to post:** Ligand-to-axial pillaring of supermolecular building layers leads to a number of isorecticular metal–organic frameworks. The copper compounds can act as hydrogen stores, and show remarkable, and selective, CO<sub>2</sub> capture.



### ■ Metal–Organic Frameworks

*K. Maity, K. Nath, M. A. Sinnwell,  
R. K. Motkuri, P. K. Thallapally, K. Biradha\**



**Isorecticular Expansion of Metal–Organic Frameworks via Pillaring of Metal Templated Tunable Building Layers: Hydrogen Storage and Selective CO<sub>2</sub> Capture**

